

Arctic Tundra Vegetation Functional Types Based on Photosynthetic Physiology and
Optical Properties

Karl F. Huemmrich^a, John Gamon^b, Craig Tweedie^c, Petya K.E. Campbell^a, David
Landis^d, Elizabeth Middleton^e

^aUniversity of Maryland Baltimore County, Code 618, Goddard Space Flight Center,
Greenbelt, MD 20771, USA, karl.f.huemmrich @ nasa.gov

^bUniversity of Alberta, Edmonton, Alberta, Canada

^cUniversity of Texas El Paso, El Paso, TX,

^dSigma Space Corp.,

^eNational Aeronautics and Space Administration

Submitted to IEEE Journal of Selected Topics in Applied Earth Observations and Remote
Sensing (J-STARS) EO-1 special issue Feb. 23, 2012

Revised December 14, 2012

Accepted February 27, 2013

1 Abstract

2 Non-vascular plants (lichens and mosses) are significant components of tundra
3 landscapes and may respond to climate change differently from vascular plants affecting
4 ecosystem carbon balance. Remote sensing provides critical tools for monitoring plant
5 cover types, as optical signals provide a way to scale from plot measurements to regional
6 estimates of biophysical properties, for which spatial-temporal patterns may be analyzed.
7 Gas exchange measurements were collected for pure patches of key vegetation functional
8 types (lichens, mosses, and vascular plants) in sedge tundra at Barrow AK. These
9 functional types were found to have three significantly different values of light use
10 efficiency (LUE) with values of 0.013 ± 0.001 , 0.0018 ± 0.0002 , and 0.0012 ± 0.0001 mol C
11 mol^{-1} absorbed quanta for vascular plants, mosses and lichens, respectively. Discriminant
12 analysis of the spectra reflectance of these patches identified five spectral bands that
13 separated each of these vegetation functional types as well as nongreen material (bare
14 soil, standing water, and dead leaves). These results were tested along a 100 m transect
15 where midsummer spectral reflectance and vegetation coverage were measured at one
16 meter intervals.

17 Along the transect, area-averaged canopy LUE estimated from coverage fractions
18 of the three functional types varied widely, even over short distances. The patch-level
19 statistical discriminant functions applied to *in situ* hyperspectral reflectance data collected
20 along the transect successfully unmixed cover fractions of the vegetation functional
21 types. The unmixing functions, developed from the transect data, were applied to 30 m
22 spatial resolution Earth Observing-1 Hyperion imaging spectrometer data to examine
23 variability in distribution of the vegetation functional types for an area near Barrow, AK.

1 Spatial variability of LUE was derived from the observed functional type distributions.
2 Across this landscape, a fivefold variation in tundra LUE was observed. LUE calculated
3 from the functional type cover fractions was also correlated to a spectral vegetation index
4 developed to detect vegetation chlorophyll content. The concurrence of these alternate
5 methods suggest that hyperspectral remote sensing can distinguish functionally distinct
6 vegetation types and can be used to develop regional estimates of photosynthetic LUE in
7 tundra landscapes.

1 Introduction

2 High northern latitudes are undergoing dramatic changes in climate. Warming
3 trends have been observed in northern regions and Global Circulation Model predictions
4 indicate arctic and boreal regions are likely to warm by several degrees over the next
5 century, a greater rate than other regions on the globe [1, 2]. In high latitudes seasonal
6 shifts in surface properties involve freezing and thawing of water, so relatively small
7 temperature changes around the freezing point can result in significant environmental
8 shifts. Along with temperature changes, significant changes in precipitation and
9 evapotranspiration are also predicted for these regions [1, 2].

10 Tundra vegetation is expected to be particularly responsive to climate change.
11 Increased warming during the growing season is likely to alter production by lengthening
12 the growing season and increasing metabolic activity [3, 4, 5]. Changes in seasonal air
13 temperature may increase soil temperatures and the active layer depth to permafrost.
14 This, in turn, affects soil microbial activity, nutrient cycles and soil moisture [6, 7], which
15 alter existing plant growth and competitive species interactions resulting in dramatic
16 changes in vegetation composition. Further, tundra ecosystems are often moisture
17 limited, so climate induced changes in precipitation patterns and surface hydrology will
18 also act to alter vegetation growth patterns [8, 9].

19 A unique characteristic of the tundra ecosystem is the relative dominance of non-
20 vascular plants in the landscape, such as mosses and lichens. In some cases, mosses
21 dominate local habitats in the tundra because of their tolerance to extreme cold,
22 dessication, water-logging, and low light [10]. Lichens can survive extreme climate
23 conditions such as drought and persistent freezing as well [11, 12, 13]. Tundra warming

manipulation experiments have shown a decline in lichens with an increase in vascular plants suggesting changing proportions of tundra plant types as climate changes [14].

Non-vascular plants can provide a significant fraction of tundra carbon uptake and should be explicitly included in descriptions of tundra carbon fluxes. Photosynthesis of tundra vascular plant canopies has been described with strong relationships found between leaf area or the fraction of absorbed photosynthetically active radiation and gross primary productivity [15, 16, 3]. However, the net primary productivity (NPP) of mosses have been shown to represent about 25-30% of total above-ground NPP in several tundra sites including; tussock tundra [9], coastal tundra [17] and tundra heath [18]. In other cases mosses were found to dominate tundra photosynthetic CO₂ fluxes [19, 20].

There are further important physiological differences between vascular and non-vascular plants that affect tundra water and energy balance. Mosses and lichens do not have roots, so cannot access soil moisture below the surface. Instead they depend on water from atmospheric humidity, ground water, or precipitation. They also do not possess stomata and therefore lose water readily to the atmosphere and many species are adapted to survive long periods of desiccation. [21]. They may also act as an insulating layer to heat transport between the soil and the atmosphere [22]. Thus, in areas where these non-vascular plants make up a significant portion of the vegetation cover the response of ecosystem carbon and energy balance to environmental changes is expected to differ from that of vascular plant-dominated vegetation and must be accounted for in tundra ecosystem modeling.

The difficulties in working in remote tundra locations have always incurred large logistical costs, therefore observations of ecosystem change using remote sensing provide

an expedient and economical method of collecting repeatable and consistent measurements over large areas. Importantly, most remote sensing theory of vegetation has been derived from studies focused on temperate crops and forests and thus the interpretation of conventional remote sensing tools is often ambiguous for northern landscapes. There are several unique features of the tundra that affect the interpretation of remotely sensed data [23]. Non-vascular plants can represent significant fractions of the tundra landscape cover, and these non-vascular plants have different spectral characteristics as well as different physiological responses from vascular plants or from bare soils [24, 25, 26]. For example, remote sensing studies have been able to detect changes in lichen-dominated areas due to responses to both short-term temperature anomalies as well as long-term temperature trends [27, 28].

This study investigates the importance of non-vascular plants in the tundra landscape and examines their effects on tundra carbon uptake, using spectral reflectance to distinguish these different functional types. We explore the concept of “optical types” [29] to scale from ground-based *in situ* measurements to landscapes using satellite observations to examine vegetation functional type patterns across the tundra.

Materials and Methods

Study Area

The study examines an area mainly located north and west of the town of Barrow, AK, including most of the Barrow Environmental Observatory. Specific study plots are located at 71° 19' 19.1" N 156° 36' 15.9" W, approximately seven kilometers east of Barrow. The area is classified as moist acidic coastal tundra [30]. Barrow has a mean

1 annual temperature of -12.0°C , with a minimum mean monthly temperature of -26.6°C
2 in February and maximum mean monthly temperature of 4.7°C in July. More than half of
3 the 106 mm of annual precipitation falls as rain during a 3-month period from July
4 through September, with the ground being snow covered from September through May to
5 mid-June [31].

6 The tundra community at Barrow, AK consists of an overstory dominated by
7 vascular plants (mostly graminoids) and an underlying mat of mosses [32]. Vascular
8 plants at Barrow include dwarf shrubs, forbs, and perennial herbs but the most dominant
9 growth form is graminoid [30]. Common vascular species are: *Carex aquatilis*, *Dupontia*
10 *fischerii*, *Eriophorum angustifolium*, *E. scheuzerii*, *Luzula confusa*, *Petasites frigidus*,
11 *Potentilla hyparctica*, and *Salix rotundifolia*. Mosses are a significant portion of the
12 community and in some areas may account for more biomass than vascular plants [33].
13 Moss species include: *Dicranum elongatum*, *D. undulatum*, *Drepanocladus revolvens*,
14 *Polytrichum (juniperum)*, and *Sphagnum* spp. Lichens are scattered throughout the drier
15 areas but are not as abundant or productive as mosses and graminoids [34] and include
16 the species: *Alectoria nigricans*, *Cetraria cucullata*, *C. nivalis*, and *Dactylina arctica*.

17

18 Measurements

19 This project included: 1) the collection of *in situ* measurements of plots for the
20 three vegetation functional types, including photosynthesis and spectral reflectance; 2)
21 measurements of ground cover amount and spectral reflectance at every meter along a
22 100 m transect; 3) development of relationships between spectral reflectance and both

1 photosynthesis and cover amount; 4) estimation of LUE across a tundra transect; and 5)
2 application of these findings to the spectral information collected from Hyperion.

3 Vegetation measurements were designed to relate photosynthetic rate to spectral
4 reflectance. Tundra vegetation were grouped into three functional groups; vascular
5 plants, mosses, and lichens, with at least four replicates per group measured on any one
6 day. Each replicate provided a different species from each group in an attempt to
7 measure the variability within a group. Field sampling for this study was conducted on
8 July 20 and August 5, 2001, near the peak of the growing season in this area.

9 Spectral reflectance measurements were collected at 51 plots, each about 15 cm in
10 diameter, representing nearly pure areas of representative tundra species. Photosynthetic
11 gas exchange measurements were collected at 17 of the plots. All of the study plots were
12 in very close proximity (<15 m) to a 100 m linear transect that was also optically sampled
13 at frequent intervals throughout the summer [35].

14 CO₂ gas exchange was measured at 17 plots where a 14.6 cm diameter collar of
15 acrylic plastic was embedded in the ground. When measurements were made, the plot
16 was enclosed in a clear acrylic chamber constructed of 0.3175 cm thick acrylic tube glued
17 to a 0.635 cm thick acrylic top and a closed gas exchange system was connected to the
18 chamber (LI-6200, LiCOR, Lincoln, NE). Each individual plot was measured under
19 ambient environmental conditions for net photosynthesis and then the measurement was
20 repeated with the chamber covered with a black cloth to block out light to provide an
21 estimate of dark respiration. Gross photosynthesis was calculated as the difference
22 between the net photosynthesis, measured with the clear chamber, and dark respiration,
23 measured with the chamber covered. A quantum sensor mounted on the chamber top

measured incident photosynthetically active radiation (PAR). The chamber had a PAR transmittance of 95% [36]. Photosynthetic light-response curves were developed using household window screen material as neutral density filters to control incident PAR, allowing photosynthesis measurements for each functional type to be rapidly collected under a range of light levels.

Light use efficiency (LUE) was determined as the ratio of absorbed light and gross photosynthesis:

$$\varepsilon = \frac{G}{f_{PAR} Q_i} \quad (1)$$

where ε is LUE, G is gross photosynthesis with units of $\mu\text{mol CO}_2 \text{ m}^{-2} \text{ s}^{-1}$, Q_i is incident PAR with units of $\mu\text{mol photons m}^{-2} \text{ s}^{-1}$ (i.e. photosynthetic photon flux density, or PPFD) and f_{PAR} is the fraction of the PAR absorbed by the vegetation (unitless). Absorbed PAR (APAR) is the product of f_{PAR} and incident PAR.

f_{PAR} is not well defined and difficult to determine for vegetation with low growth forms such as lichens and mosses. We assumed that no PAR was transmitted through moss and lichen mats, so for these vegetation types f_{PAR} is 1-PAR albedo. PAR albedo is estimated by integrating the measured spectral reflectance (see below) between 400 and 700 nm. For the vascular plant plots f_{PAR} is determined using the linear relationship between Normalized Difference Vegetation Index (NDVI) and f_{PAR} described in Huemmrich et al. [36].

Optical Sampling

1 The optical field sampling consisted of measurements of the small single species
2 plots, as well as measurements collected at every meter along a 100 m transect to observe
3 areas of mixed coverage [35, 37, 38]. Optical measurements were collected using two
4 portable field spectrometers (UniSpec, PP Systems, Haverhill, MA). These
5 spectrometers measured reflectance between 310 and 1130 nm sampling at approximately
6 3 nm intervals.

7 For plot measurements, the spectrometer was fitted with a glass fiber optic cable
8 connected to a stainless steel ferrule, which provided a 20° field of view. Reflected
9 irradiance measurements were collected with the end of the fiber optic cable held
10 vertically between 30 and 40 cm above the surface to view an area of less than 15 cm
11 diameter to match the area of gas exchange measurements. Within seconds of collecting
12 a surface measurement, a reference measurement was made of a calibration panel
13 (Spectralon, Labsphere, Inc. North Sutton, NH). The speed of this procedure allowed the
14 acquisition of data even under cloudy conditions. Three reflectance spectra were
15 collected for each sampled plot, and were averaged to produce one spectrum per plot. In
16 addition to the vegetation plots, spectral measurements for nongreen materials including
17 bare soil, open water, and areas of standing dead vascular plants, were collected soon
18 after snowmelt and before the start of green-up. For the vegetation plots, ground-based
19 spectral reflectance measurements were collected near the height of peak productivity
20 period in early August (August 5 and 8, 2001) and reflectance for nongreen plots were
21 collected throughout the summer (June 20 and 30, July 15, August 8 and 22, and
22 September 3, 2001).

1 To characterize spectral reflectance patterns at multiple spatial scales, spectral
2 measurements were made at 1 m intervals along a 100 m linear track system [35, 38].
3 The track was supported less than a meter above the tundra surface by tripods with a tram
4 cart riding on the track carrying a dual channel spectroradiometer (Unispec DC, PP
5 Systems). From the spectrometer were two fiber-optic cables mounted on a mast and
6 boom attached to the cart, one attached to a diffuser head viewing upward, the other on
7 the boom pointing vertically downward to view an area south of the track with a field-of-
8 view of approximately 1 m in diameter. With each measurement of reflected radiance, a
9 measurement of incident irradiance was also acquired at the same time for a
10 determination of surface reflectance. Due to the coincident measurements of both
11 incoming and reflected radiation this system was able to correct for effects of varying
12 cloud cover. The tram system collected spectral measurements that were repeatable
13 throughout the growing season while minimizing disturbance to the tundra surface [35,
14 38]. In this study we used measurements from the peak of the growing season period
15 collected on August 10, 2001.

16 Processing the ground-measured spectral reflectance data included interpolating
17 the spectral bands to 1 nm intervals. Due to instrument noise at the ends of the
18 spectrometer range, the usable spectral range was between 400 and 1000 nm. The
19 processing used freely available software (Multispec v.4.0,
20 http://specnet.info/specnet_toolkit.htm). The spectral reflectance data were then
21 convolved to match the approximately 11 nm band passes of the Hyperion instrument
22 [39] in subsequent analyses.

1 Imaging spectrometer data were acquired on July 20, 2009 (day 201) by the
2 Hyperion instrument on the Earth Observing-1. Hyperion provides data in 220 spectral
3 bands from 0.4 to 2.5 μm at 30-meter resolution and a 7.5 km wide swath [39]. The
4 satellite data were atmospherically corrected to surface reflectance using the Atmosphere
5 Removal algorithm (ATREM) [40, 41]. To match the spectral range of the ground-based
6 spectral data only 55 of the continuous Hyperion bands between 437 and 993 nm were
7 used.

8 Discriminant analysis was used to separate the functional groups based on optical
9 properties, determining the important spectral bands and simplifying the number of
10 independent variables [42]. The plot data were divided into four groups: vascular plants,
11 mosses, lichens, and nongreen materials (bare soil, dead vegetation, and standing water).
12 Inputs to the discriminant analysis using Systat (Version 13, Systat Software, Inc.,
13 Chicago, IL) were plot reflectance spectra convolved to the Hyperion bands. The
14 analysis used a forward stepwise method (Wilks' Lamda) to test for significant mean
15 group differences, using a probability of $F \leq 0.05$ to include bands and $F \geq 0.10$ to remove
16 the band.

17 At each meter along the 100 m transect a visual estimate of species abundance
18 was made over the period August 8-11, 2001 using a 1 m by 1 m quadrat. The species
19 data were converted into percent area of each of the vegetation functional types and
20 nongreen material types. We estimate errors in the estimation of coverage to be +/- 15%
21 cover. Because of the three dimensional structure of the vegetation the sum of the
22 coverage was more than 100%. For this analysis, the total measured cover values were

normalized so total cover equals 100% as is generally done in linear unmixing approaches.

LUE was determined for areas with mixtures of different functional types as the weighted sum of the LUE from the pure plots, where the weight coefficients were the normalized fractional cover values. This calculation assumes that the incident PAR is absorbed by the landscape components proportional to their normalized cover fraction and was applied to determine LUE for both the transect data and the Hyperion satellite imagery.

Chlorophyll concentrations are a key physiological factor related to maximum photosynthetic rates. We estimated chlorophyll concentrations using Gitelson's three-band model:

$$C_i = \left(\frac{1}{\rho_{\lambda_1}} - \frac{1}{\rho_{\lambda_2}} \right) \rho_{\lambda_3} \quad (2)$$

where the spectral index C_i is proportional to the chlorophyll concentration, and ρ_{λ} is the reflectance for a given wavelength band, λ . Wavelengths chosen are maximally sensitive to absorption by chlorophyll and other pigments ($\lambda_1=549$ nm), are influenced primarily by non-chlorophyll pigments ($\lambda_2=793$ nm), and where reflectance is controlled by leaf scattering ($\lambda_3=793$ nm) [43, 44, 45].

The cover estimates of the functional types retrieved from the Hyperion imagery were used to derive landscape LUE patterns. The LUE per pixel was calculated as described above and compared with chlorophyll concentration estimates obtained using Equation 2.

Results

1 The physiological measurements identify differences relating to photosynthetic
2 carbon exchange among the three vegetation functional types. From the plot gas
3 exchange data, LUE for each functional type was calculated as the slope of a linear
4 regression between gross photosynthesis and APAR, forced through the origin (Figure 1,
5 Table 1). Lichens, mosses, and vascular plants all had different LUE values. Vascular
6 plants had significantly higher net photosynthetic rates and LUE than the other two
7 functional types. The vascular plant LUE from this study ($0.0134 \text{ mol C mol}^{-1} \text{ quanta}$)
8 was close to that previously determined for a vascular plant overstory near Barrow
9 ($\text{LUE}=0.0126 \text{ mol C mol}^{-1} \text{ quanta}$ [36]) and within the 95% confidence interval of the
10 slope from the regression in this study (i.e. the vascular plant LUE). This was noteworthy
11 as the LUE in this study was based only on measurements collected during the middle of
12 the growing season, while the Huemmrich et al. [36] LUE was derived from
13 measurements collected throughout the growing season, suggesting the LUE for vascular
14 plants was relatively stable over much of the season, as well as having similar LUE
15 values for vascular plants in mixtures with mosses or growing alone.

16 The LUE for mosses and lichens were much lower than for vascular plants. There
17 was a significant difference, however, between these two functional types (Table 1) with
18 mosses having a LUE almost 50% greater than lichens (a similar analysis for LUE of the
19 moss data was presented in [36]).

20 The *in situ* spectral reflectance measurements of the plots were divided up into
21 four groups: vascular plants ($n=22$), mosses ($n=11$), lichens ($n=18$), and nongreen
22 material ($n=19$) (Figure 2). Generally, the vascular plant and moss spectra were similar,
23 and display typical green plant spectral reflectance patterns, including more variation in

1 the near infrared than in visible wavelengths. In comparison, lichen spectra had much
2 higher visible reflectance and were more variable in all wavelengths. Spectral patterns for
3 the nongreen materials were clearly different for dead vegetation, bare soil, and water.
4 Generally the spectral variability for the entire nongreen group increases as a function of
5 wavelength.

6 Discriminate analysis provided an objective tool to evaluate the ability of optical
7 sampling to distinguish functional groups and to identify a subset of the spectral bands to
8 do this separation. The stepwise method for discriminate analysis reduced the number of
9 wavebands from 55 to five, yet retained separation of functional types. The five chosen
10 bands were located in key locations of typical green plant spectra (Figure 2); at the blue
11 (488 nm) and red (671 nm) chlorophyll absorption wells, near the inflection point of the
12 red edge (712 nm), at the shoulder of the red edge (763 nm), and in the near infrared
13 “plateau” (834 nm). Mulhern [46] identified the blue band as an important spectral region
14 for separating lichens from soils. The discriminate analysis functions (Figure 3) correctly
15 predicted 83% of group membership overall, with 86% correct for vascular plants, 91%
16 for mosses, 95% for the nongreen materials, and 61% for lichens. Lichen errors were
17 mainly due to confusion with the nongreen materials (Figure 3).

18 Even at the scale of one square meter, the cover estimates along the tram transect
19 show that all square meter plots consisted of mixtures of multiple cover types (Figure 4).
20 The observed cover estimates included little bare ground with maximum coverage of
21 20%, while standing dead vegetation ranged from 0-70%, and water from 0-100%. Moss
22 coverage ranged from 0-100%, but when normalized to a 100% maximum total coverage
23 maximum moss coverage was 40% +/- 7%, based on the propagation of an assumed 15%

error in the original observations. Lichen coverage ranged from 0-90% with 35% \pm 7% maximum normalized lichen coverage. Vascular plant coverage ranged between 40-150%, with normalized coverage of 18-88% \pm 9%. Vascular plant coverage was highest in the locally low areas, particularly the areas with standing water, while moss coverage was highest in locally low areas without standing water and on the edges of the wet areas. Lichen coverage was highest in the locally high areas where bare soil patches also occurred. These spatial patterns indicate the role of microtopography on the distribution of the functional types.

The transect coverage observations indicate how heterogeneous the tundra is, as areas over a few square centimeters in size generally consist of mixtures of multiple types. Therefore, to estimate LUE at that scale of a 30 m Hyperion pixel, the fractions of each functional type must be determined. We used the optical measurements to scale from plot-level LUE to 30 m areas. Since the discriminant functions optimized separation of the different functional types with a small number of spectral bands, we used the distance to endmembers in the discriminate analysis function space to estimate cover fractions in mixed pixels. Assuming that the range of *in situ* plot reflectances provide a reasonable description of the variability of plot type, the endmembers for the moss, lichen, and nongreen cover types were assigned values of the average of the plot reflectances. However, variability in the vascular plants reflectance is driven by differences in green leaf area index. To account for that variability the vascular plant endmember was chosen to be the “greenest” plot spectra (i.e. spectra with the highest NDVI, which was also the greatest distance from the average of all the plot values in the discriminate analysis function space).

Endmember reflectance for each functional type and reflectances at each meter along the transect were transformed using the discriminate analysis functions. The distances in the discriminate analysis space between the coverage estimates for each square meter and the endmembers were calculated, these were related to the observed coverage to create transfer functions. The statistical associations between distance from endmembers and observed coverage were low due to large observation errors relative to the range of values, with R^2 values of 0.39, 0.13, and 0.19 for vascular plants, mosses, and lichens respectively. Nevertheless, the cover fractions determined from the *in situ* reflectance were found to be in close agreement with sampled cover fractions (Figure 6), with root mean square error (RMSE) of 11% cover for vascular plants, 8% for moss, 9% for lichen, and an overall RMSE of 9% cover.

LUE was calculated for each square meter block along the transect using the observed cover fraction and coverage estimated from the reflectance spectra (Figures 5 and 7). Along the transect LUE was quite variable, with maximum and minimum values occurring within 6 m of each other (Figure 7). Variability in LUE was affected by microtopography, with higher values of LUE tending to occur in locally low, wet areas. This variability over the 100 m distance produced a fourfold difference in LUE with values from 0.003 to 0.012 mol C mol⁻¹ quanta for the *in situ* observations. The average errors for estimating LUE were similar for the two methods: 0.0014 mol C mol⁻¹ quanta for the method using observed coverage and 0.0015 mol C mol⁻¹ quanta for the LUE based on the remote sensing approach. The two different LUE calculations have a correlation of 0.62 with a RMSE of 0.0013 mol C mol⁻¹ quanta.

1 The equations relating spectral reflectance and functional type coverage derived
2 from the transect data were the applied to the Hyperion imagery to create a continuous
3 fields description of the coverage of the functional types for the tundra around Barrow
4 (Figure 8b). Over this area the distribution of vascular plant coverage per pixel had a
5 maximum value of 74% with a distribution peak of 32%, for mosses the maximum
6 coverage was 31% with the distribution peak at 22%, and for lichens the maximum
7 coverage was 22% with a peak of 10%.

8 Without ground observations of vegetation type coverage, an examination of an
9 area known to be free of vegetation was used to make an error estimate. The old Naval
10 Arctic Research Laboratory runway was chosen as for this test. For runway pixels
11 vascular plant coverage was as high as 9%, moss 14%, and lichen 13%, compared to
12 expected values of zero percent coverage. These values were close to the RMSE of
13 coverage from the tram analysis comparing the spectral unmixing with ground
14 observations, suggesting the Hyperion unmixing captured the actual functional type
15 distribution near this level of error.

16 There are clearly observed spatial patterns in the cover fractions in this landscape.
17 High vascular plant coverage occurred on the margins of drained lakes. Higher lichen
18 coverage tended to be found in drier upland regions. This pattern of lichen occurrence
19 was also observed in the transect measurements (figure 4). Moss coverage was more
20 widely distributed, although high moss coverage in the middle of the drained lakes may
21 be erroneous due to confusion between mosses and mixtures of water and vascular plants.
22 Field observations confirm that moss often occurs as a low, “background” layer beneath
23 the vascular canopy of wet tundra in this region [36].

1 The Hyperion functional type coverage estimates were used to calculate landscape
2 patterns of LUE (Figure 8c). For the vegetated parts of the scene, this Hyperion-based
3 LUE ranged from 0.0021-0.0102 mol C mol⁻¹ quanta, a fivefold difference between
4 maximum and minimum LUE. The distribution peak of LUE for this area and the overall
5 average were both 0.0048 mol C mol⁻¹ quanta.

6 The Hyperion-based LUE was compared with the chlorophyll spectral index, Ci
7 (Equation 2). Ci was well correlated with LUE over the study area ($R^2=0.69$, $SE=0.0006$
8 mol C mol⁻¹ quanta) (Figure 9) suggesting vegetation chlorophyll concentration is a key
9 determinant of LUE for this tundra ecosystem. This suggests that a more direct approach
10 for deriving spatial patterns of LUE for tundra from imaging spectrometry would be
11 based on a simple reflectance-based metric of chlorophyll concentration.

12

13 Discussion and Conclusions

14 This study uses the concept of optical types [29] to examine a key characteristic
15 of ecosystem carbon exchange in the tundra. To have usable optical types one must be
16 able to both identify significant functional differences in vegetation types and spectrally
17 identify these different types. Our grouping of tundra vegetation (vascular plants, mosses,
18 and lichens) meets these criteria. Among the different types, the plot measurements
19 showed distinct differences in LUE, a key variable describing photosynthetic carbon
20 uptake and discriminate analysis showed that the types could be separated based on their
21 spectral reflectance. The ability to link LUE to reflectance characteristics provides an
22 approach to scale from the ground measurements to distributions over a landscape. Using
23 an unmixing approach we were able to create continuous fields of key tundra functional

1 types for this area, an improvement over simple classifications. Results from this study
2 demonstrated how, even at a scale of a square meter, variable mixtures of functional
3 types produced significantly different values for LUE. Unmixing using spectral
4 reflectance provides a unique estimate of LUE for each pixel. Remote sensing provides a
5 way to map large areas and make noninvasive repeat measurements to monitor ecosystem
6 change. Remote sensing is a particularly important tool for observing tundra due to the
7 difficulties and expense involved in traveling to and working in this region, rendering
8 direct field sampling over large areas impractical.

9 The linear unmixing approach used to calculate pixel-level LUE simplifies the
10 tundra canopy as it does not take into account the three dimensional structure of a
11 vascular plant overstory. Vascular plants can grow through mats of mosses and lichens
12 and shade them, decreasing their photosynthetic production [36]. However, vascular plant
13 leaf area index for this region is generally low, with observed midseason values less than
14 2 [36]. We believe the overall effect of this overstory on the moss and lichen understory
15 production is relatively small in this region due to both the low leaf area combined with
16 generally diffuse light conditions.

17 This study provided a snap-shot of this landscape at a particular point in time.
18 Seasonal growth of vascular plants will change their relative proportions throughout the
19 growing season and this affects carbon uptake and LUE patterns [38]. Early in the
20 growing season, as vascular plants begin to grow, tundra productivity will be dominated
21 by moss and lichen photosynthesis, with the vascular plant component increasing as the
22 season progresses [36]. Thus, the spatial patterns of coverage and LUE are expected to
23 change through the growing season.

1 The correlation between LUE calculated from coverage estimates and the
2 chlorophyll index (Ci), even though they use different algorithms and spectral bands,
3 demonstrates how multiple approaches can yield similar results. This convergence is
4 most likely due to plant physiological constraints indicating chlorophyll concentration is
5 a controlling factor in vegetation photosynthetic efficiency, and may provide a more
6 direct approach to deriving LUE.

7 This study found significant variability in functional type cover fractions, leading
8 to variability in estimated LUE, at local scales (meters) in the field data collected along
9 the transect and at landscape scales (km) in the satellite imagery. The spatial variability
10 shown in LUE estimates is not accounted for in existing carbon flux models. Spatial
11 distributions of vegetation functional types were strongly related to surface
12 microtopography, from which we infer surface hydrology to be a significant controlling
13 factor. These results suggest that climate change affecting surface hydrology [47] will
14 also affect spatial patterns of vegetation distribution and ecosystem carbon exchange.
15 Particularly in a scenario of modified surface hydrology, we can expect that climate
16 change will affect relative coverage due to differing responses of each of the functional
17 types to climate change, and that these changes in cover will be associated with altered
18 carbon and energy balance.

19 Since hydrology is an important factor determining the vegetation functional type
20 coverage, shortwave infrared bands may provide additional information on vegetation
21 water content, improving the retrieval of functional type coverage [48]. This approach
22 was not tested in this study as the field measurements observed only visible and near
23 infrared spectral bands. Recent observations combining NIR and blue bands to detect

1 standing water in coastal tundra [49] may also prove useful at detecting hydrological
2 changes linked to cover type and LUE.

3 The results of this study are indicative only of this part of the Alaskan coastal
4 tundra and further field studies are required in other parts of the tundra biome to test and
5 extend the results and to evaluate the ability to generalize the results. For example, shrubs
6 are an important component of the tundra biome and shrub coverage has been shown to
7 be increasing in the tundra [50]. Shrubs did not represent a significant cover type in our
8 study area, however, so were not explicitly included in this study. Future work is required
9 to examine shrub optical and physiological characteristics to see if they comprise an
10 optically distinct functional type.

11 The use of multiple narrow spectral bands for the unmixing points to an application
12 for the future NASA Hyperspectral Infrared Imager (HyspIRI) mission for mapping
13 tundra vegetation distribution according to physiological function, hydrology, and
14 microtopography over the entire biome. The concept of optical types (optically
15 distinguishable functional types) may prove to be useful for this kind of functional
16 mapping. Similarly, simple metrics of surface water cover (e.g. [49]) or pigment
17 distribution (e.g. [45]) may provide insight into the proximal causes of functional change
18 in tundra ecosystems.

19 The close linking of optical properties and carbon flux measurements in this study
20 has provided insights into the functioning of the tundra ecosystem by identifying fine-
21 scale patterns of LUE that may be related to hydrology and microtopography. This study
22 also illustrates new “scaleable” functional mapping techniques that can be extended
23 through the use of satellite remote sensing to larger regions. This approach lends itself to

1 future studies considering how species composition relates to changing ecosystem
2 function and provides a framework for studying ecosystem change through remote
3 sensing that considers shifts in hydrology, species composition, and their effects on
4 carbon balance.

5

6 **Acknowledgements**

7 Funding for the field component of this study was provided by IARC to J. Gamon
8 and K.F. Huemmrich through the Desert Research Institute, Reno, Nevada. The authors
9 thank Stan Houston and Erika Anderson for their work on the field data collection.
10 Thanks also to Glen Kinoshita, Hyojung Kwon, Rommel Zulueta, Joe Verfaillie, and Bob
11 Hollister for their help and friendship in the field; and the staff of BASC (Barrow Arctic
12 Science Consortium) for logistics support.

13

1 **References**

- 2 [1] ACIA, *Impacts of a warming Arctic: Arctic climate impact assessment*. Cambridge
3 University Press, Cambridge, 2005.
- 4 [2] IPCC, *Climate Change 2007: The Physical Science Basis. Contribution of Working*
5 *Group I to the Fourth Assessment Report of the Intergovernmental Panel on*
6 *Climate Change*. S. Solomon, D. Qin, M. Manning, Z. Chen, M. Marquis, K.B.
7 Averyt, M. Tignor and H.L. Miller, Eds. Cambridge University Press, Cambridge,
8 United Kingdom and New York, NY, USA, 2007.
- 9 [3] K.F. Huemmrich, G. Kinoshita, J.A. Gamon, S. Houston, H. Kwon, and W.C. Oechel,
10 “Tundra Carbon Balance Under Varying Temperature and Moisture Regimes,”
11 *Journal of Geophysical Research*, vol. 115, no. G00I02, doi.
12 10.1029/2009JG001237, 2010.
- 13 [4] E.R. Humpreys, and P.M. LaFleur, “Does earlier snowmelt lead to greater CO₂
14 sequestration in two low Arctic tundra ecosystems?” *Geophysical Research Letters*,
15 vol. 38, no. L09703, doi. L09703, doi:10.1029/2011GL047339, 2011.
- 16 [5] M. Jahn, T. Sachs, T. Mansfeldt, and M. Overesch, “Global climate change and its
17 impacts on the terrestrial Arctic carbon cycle with special regards to ecosystem
18 components and the greenhouse-gas balance,” *Journal of Plant Nutrition and Soil*
19 *Science*, vol. 173, pp. 627-643, 2010.
- 20 [6] M.T. van Wijk, K.E. Clemmensen, G.R. Shaver, M. Williams, T.V. Callaghan, F.S.
21 Chapin, J.H.C. Cornelissen, L. Gough, S.E. Hobbie, S. Jonasson, J.A. Lee, A.
22 Michelsen, M.C. Press, S.J. Richardson, and H. Rueth, “Long-term ecosystem level
23 experiments at Toolik Lake, Alaska, and at Abisko, Northern Sweden:

- 1 generalizations and differences in ecosystem and plant type responses to global
2 change,” *Global Change Biology*, vol. 10, no. 1, pp. 105-123, 2004.
- 3 [7] E.A.G. Schuur, et al. “Vulnerability of permafrost carbon to climate change:
4 Implications for the global carbon cycle,” *BioScience*, vol. 58, no. 8, pp. 701–714,
5 2008.
- 6 [8] L.C. Bliss, J. Svoboda, and D.I. Bliss, “Polar deserts, their plant cover and plant-
7 production in the Canadian High Arctic,” *Holarctic Ecology*, vol. 7, pp. 305-324,
8 1984.
- 9 [9] F.S. Chapin, G.R. Shaver, A.E. Giblin, K.J. Nadelhoffer, and J.A. Laundre,
10 “Responses of Arctic tundra to experimental and observed changes in climate,”
11 *Ecology*, vol. 76, pp. 694–711, 1995.
- 12 [10] L.L. Tieszen, P.C. Miller, and W.C. Oechel, “Photosynthesis,” in *An arctic*
13 *ecosystem: The coastal tundra at Barrow, Alaska*, J. Brown, P.C. Miller, L.L.
14 Tieszen, and F.L. Bunnell, Eds. Dowden, Hutchinson, and Ross, Inc. Stroudsburg.
15 pp. 120-139, 1980.
- 16 [11] L. Kappen, “Response to extreme environments,” in *The Lichens*, V. Ahmadjian and
17 M.E. Hale, Eds. Academic Press, New York, pp. 311-380, 1974.
- 18 [12] D.H.S. Richardson, “Photosynthesis and carbohydrate movement,” in *The Lichens*,
19 V. Ahmadjian and M.E. Hale, Eds. Academic Press, New York, pp. 251-288, 1974.
- 20 [13] K.A. Kershaw, “Photosynthetic capacity changes in lichens and their potential
21 ecological significance.” in *Lichen Physiology and Cell Biology*, D.H. Brown Ed.
22 Plenum Press, New York, pp. 93-109, 1984.

- [14] J.H.C. Cornelissen, T.V. Callaghan, J.M. Alatalo, A. Michelsen, E. Graglia, A.E. Hartley, “Global change and Arctic ecosystems: Is lichen decline a function of increases in vascular plant biomass?” *Journal of Ecology*, vol. 89, pp. 984–994, 2001.
- [15] L.E. Street, G.R. Shaver, M. Williams, M.T. Van Wijk, “What is the relationship between changes in canopy leaf area and changes in photosynthetic CO₂ flux in arctic ecosystems?” *Journal of Ecology*, vol. 95, pp. 139–150, 2007.
- [16] G.R. Shaver, L.E. Street, E.B. Rastetter, M.T. Van Wijk, M. Williams, “Functional convergence in regulation of net CO₂ flux in heterogeneous tundra landscapes in Alaska and Sweden.” *Journal of Ecology*, vol. 95, pp. 802–817, 2007.
- [17] P.C. Miller, P.J. Webber, W.C. Oechel, and L.L. Tieszen, “Biophysical processes and primary production,” in *An Arctic Ecosystem: the Coastal Tundra at Barrow, Alaska* J.M. Brown, P.C. Miller, L.L. Tieszen, and F.L. Bunnell Eds., Dowden, Hutchinson & Ross, Inc., Stroudsburg, PA, pp. 66–101, 1980.
- [18] M. Campioli, R. Samson, A. Michelsen, S. Jonasson, R. Baxter, and R. Lemeur, “Nonvascular contribution to ecosystem NPP in a subarctic heath during early and late growing season,” *Plant Ecology*, vol. 202, pp. 41–53, 2009.
- [19] J. Douma, M.T. van Wijk, S.I. Lang, and G.R. Shaver, “The contribution of mosses to the carbon and water exchange of arctic ecosystems: quantification and relationships with system properties,” *Plant, Cell and Environment*, vol. 30, pp. 1205–1215, 2007.

- [20] L.E. Street, P.C. Stoy, M. Sommerkorn, B.J. Fletcher, V.L. Sloan, T.C. Hill, M. Williams, “Seasonal bryophyte productivity in the sub-Arctic: a comparison with vascular plants,” *Functional Ecology*, vol. 26, pp. 365–378, 2012.
- [21] M.C.F. Proctor, “The bryophyte paradox: tolerance of desiccation, evasion of drought,” *Plant Ecology*, vol. 151, pp. 41–49, 2000.
- [22] J. Beringer, A.H. Lynch, F.S. Chapin, M. Mack, and G.B. Bonan, “The representation of arctic soils in the land surface model: the importance of mosses,” *Journal of Climate*, vol. 14, pp. 3324–3335, 2001.
- [23] A. Hope and D. Stow, “Shortwave Reflectance Properties of Arctic Tundra,” in *Landscape Function and Disturbance in Arctic Tundra*, J. Reynolds and J. Tenhunen Eds. Ecological Studies, Vol. 120. Heidelberg: Springer-Verlag, 1995.
- [24] W.G. Rees, O.V. Tutubalina, and E.I. Golubeva, “Reflectance spectra of subarctic lichens between 400 and 2400 nm,” *Remote Sensing of Environment*, vol. 90, pp. 281–292, 2004.
- [25] D.E. Petzold D.E. and S.N. Goward, “Reflectance spectra of subarctic lichens,” *Remote Sensing of Environment*, vol. 24, pp. 481–492, 1988.
- [26] J.E. Vogelmann and D.M. Moss, “Spectral reflectance measurements in the genus *Sphagnum*,” *Remote Sensing of Environment*, vol. 45, pp. 273–279, 1993.
- [27] I. Olthof and R. Latifovic, “Short-term response of arctic vegetation NDVI to temperature anomalies,” *International Journal of Remote Sensing*, vol. 28, pp. 4823–4840, 2007.

- [28] I. Olthof and D. Pouliot, “Treeline vegetation composition and change in Canada's western Subarctic from AVHRR and canopy reflectance modeling,” *Remote Sensing of Environment*, vol. 114, no. 4, pp. 805–815, 2010.
- [29] S.L. Ustin and J.A. Gamon, “Remote sensing of plant functional types,” *New Phytologist*, vol. 186, pp. 795–816, 2010.
- [30] J. Brown, K.R. Everett, P.J. Webber, S.F. MacLean Jr, and D.F. Murray, “The coastal tundra at Barrow,” in *An Arctic Ecosystem, The Coastal Tundra at Barrow, Alaska*, J. Brown, P.C. Miller, L.L. Tieszen and F.L. Bunnell, Eds. Dowden, Hutchison, and Ross, Stroudsburg, Pennsylvania, pp. 1-29, 1980.
- [31] K.M. Hinkel, F.E. Nelson, A.E. Klene and J.H. Bell, “The Urban heat island in winter at Barrow, Alaska,” *International Journal Of Climatology*, vol. 23, pp. 1889–1905, 2003.
- [32] L.C. Bliss, “The evolution and characteristics of tundra,” in *Tundra Ecosystems: a Comparative Analysis*, L.C. Bliss, O.W. Heal and J.J. Moore, Eds. Cambridge University Press, Cambridge, pp. 5-46, 1981.
- [33] P.J. Webber, P.C. Miller, F.S. Chapin III, and B.H. McCown, “The Vegetation: pattern and succession,” in *An Arctic Ecosystem, The Coastal Tundra at Barrow, Alaska*, J. Brown, P.C. Miller, L.L. Tieszen, and F.L. Bunnell Eds., Dowden, Hutchison, and Ross, Stroudsburg, PA, pp. 186-218, 1980.
- [34] F.E. Wielgolaski, L.C. Bliss, J. Svoboda, and G. Doyle, “Primary production of tundra,” in *Tundra Ecosystems: a Comparative Analysis*, L.C. Bliss, O.W. Heal and J.J. Moore, Eds. Cambridge University Press, Cambridge, pp. 187-225, 1981.

- [35] D.A. Stow, A. Hope, D. McGuire, et al. "Remote sensing of vegetation and land-cover change in Arctic tundra ecosystems," *Remote Sensing of Environment*, vol. 89, pp. 281-308, 2004.
- [36] K.F. Huemmrich, J.A. Gamon, C.E. Tweedie, S.F. Oberbauer, et al. "Remote sensing of tundra gross ecosystem productivity and light use efficiency under varying temperature and moisture conditions," *Remote Sensing of Environment*, vol. 114, no. 3, pp. 481-489, 2010.
- [37] J.A. Gamon, Y. Cheng, H. Claudio, L. MacKinney, and D. Sims, "A mobile tram system for systematic sampling ecosystem optical properties," *Remote Sensing of Environment*, vol. 103, pp. 246-254, 2006.
- [38] J.A. Gamon, K.F. Huemmrich, R.S. Stone, C.E. Tweedie, "Spatial and temporal variation in primary productivity (NDVI) of coastal Alaskan tundra: Decreased vegetation growth following earlier snowmelt." *Remote Sensing of Environment*, vol. 129, pp. 144–153, 2013.
- [39] S.G. Ungar, J.S. Pearlman, J.A. Mendenhall, and D. Reuter, "Overview of the Earth Observing One (EO-1) mission," *IEEE Transactions on Geoscience and Remote Sensing*, vol. 41, no. 6, pp. 1149-1159, 2003.
- [40] B.-C. Gao, K.B. Heidebrecht, and A.F.H. Goetz, "Derivation of scaled surface reflectances from AVIRIS data," *Remote Sensing of Environment*, vol. 44, pp. 165-178, 1993.
- [41] B.-C. Gao, M.J. Montes, C.O. Davis, and A.F.H. Goetz, "Atmospheric correction algorithms for hyperspectral remote sensing data of land and ocean," *Remote Sensing of Environment*, vol. 113, Supplement 1, pp. S17-S24, 2009.

- [42] W.R. Klecka, *Discriminant Analysis*, Sage Publications, Inc., Newbury Park, CA, USA, 1980.
- [43] A.A. Gitelson, G.P. Keydan, and M.N. Merzlyak, “Three-band model for non-invasive estimation of chlorophyll, carotenoids, and anthocyanin contents in higher plant leaves,” *Geophysical Research Letters*, vol. 33, pp. L11402, 2006.
- [44] S.L. Ustin, A.A. Gitelson, S. Jacquemoud, M. Schaepman, G.P. Asner, J. A. Gamon, and P. Zarco-Tejada, “Retrieval of foliar information about plant pigment systems from high resolution spectroscopy,” *Remote Sensing of Environment*, vol. 113, pp. S67–S77, 2009.
- [45] A.A. Gitelson, “Nondestructive estimation of foliar pigment (chlorophylls, carotenoids, and anthocyanins) contents: Evaluating a semianalytical three-band model” in *Hyperspectral Remote Sensing of Vegetation*, P.S. Thenkabail, J.G. Lyon, and A. Huete, Eds. Taylor and Francis, 2011.
- [46] T. Mulhern, “Spectral contrasts of subarctic vegetation: basis for mapping lichens with satellite data,” PhD dissertation, University of Maryland at College Park, 1995.
- [47] L.C. Smith, Y. Sheng, G.M. MacDonald, and L.D. Hinzman,” Disappearing Arctic lakes.” *Science*, vol. 308, pp. 1429, 2005.
- [48] C. Roberto, B. Lorenzo, M. Michele, R. Micol, and P. Cinzia, “Optical remote sensing of vegetation water content” in *Hyperspectral Remote Sensing of Vegetation*, P.S. Thenkabail, J.G. Lyon, and A. Huete, Eds. Taylor and Francis, 2011.

- 1 [49] S. Goswami, J.A. Gamon, and C.E. Tweedie, “Surface hydrology of an arctic
2 ecosystem: multi-scale analysis of a flooding and draining experiment using
3 spectral reflectance,” *J. Geophys. Res.*, vol. 116, no. G00I07, doi
4 10.1029/2010JG001346, 2010.
- 5 [50] M. Sturm, C. Racine, and K. Tape, “Increasing shrub abundance in the Arctic,”
6 *Nature*, vol. 411, pp. 546-547, 2001.
- 7

1 **Tables**

2

	Vascular Plants	Moss	Lichen
LUE	0.01337	0.00184	0.00124
St. Err. of Slope	0.00101	0.00022	0.00011
Num. Obs.	29	25	28
R ²	0.74	0.56	0.74
P	<0.01	<0.01	<0.01

3 Table 1. Light Use Efficiency based on regressions between net photosynthesis and

4 APAR from plot data. LUE is in units of mol C mol⁻¹ absorbed quanta.

5

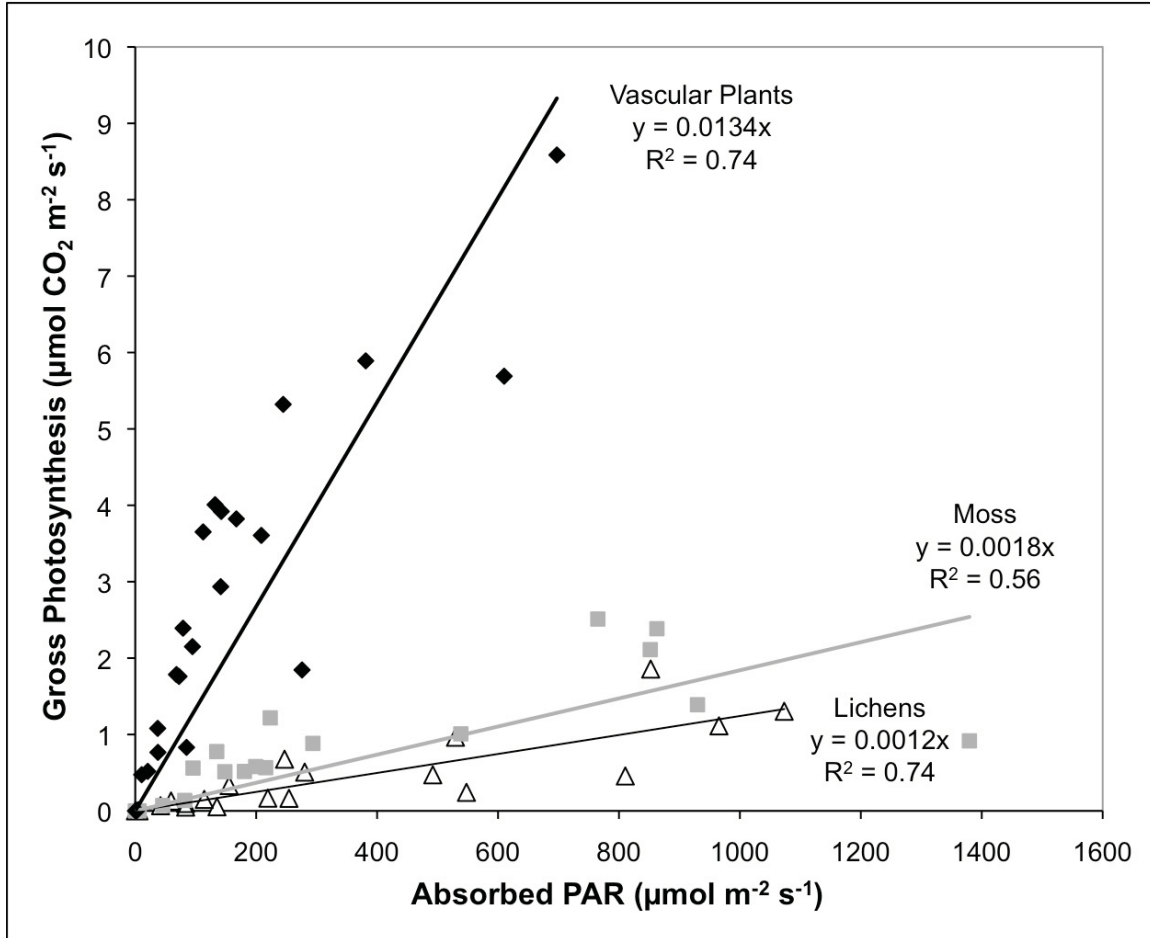
	Vascular Plants	Moss	Lichen
R ²	0.39	0.13	0.19
P	<0.01	<0.01	<0.01
Est. Obs. Error	9.5	7.1	7.0
SE of Regression	10.8	8.4	9.0

6 Table 2. Description of relationships in spectral space between the statistical distance to

7 endmembers and coverage estimate observations, acquired along the tram transect. The

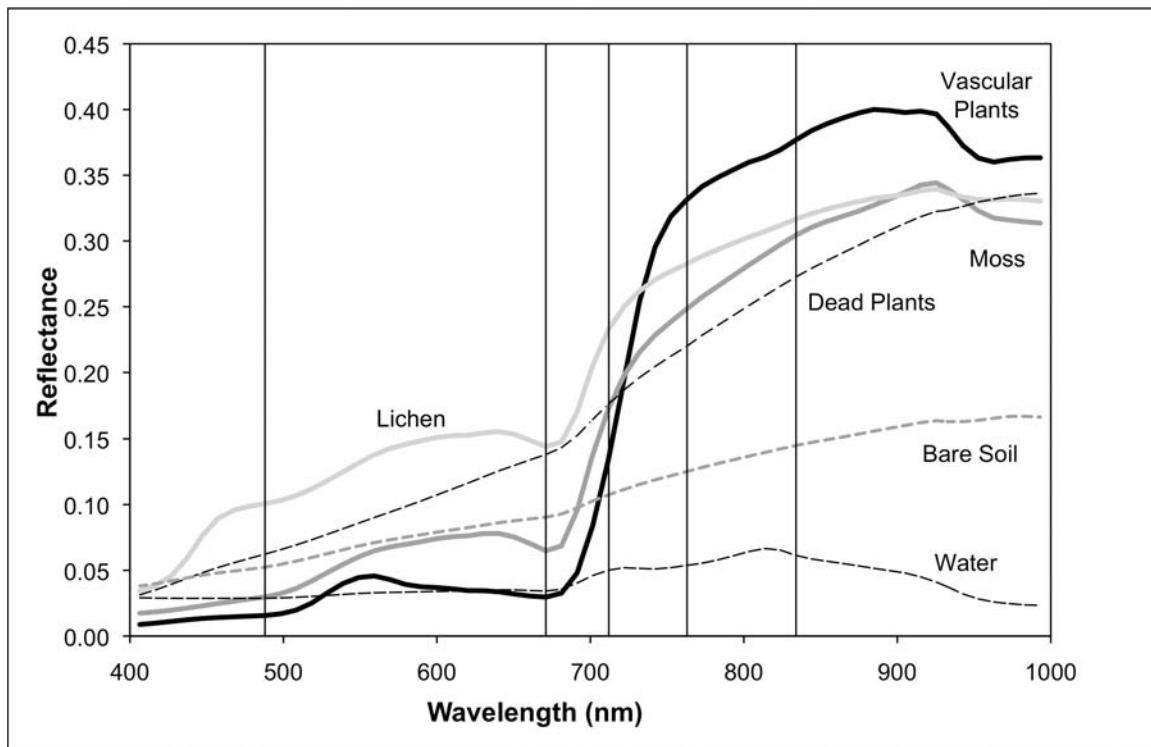
8 errors are expressed in percent coverage. For all cases the number of observations is 100.

9

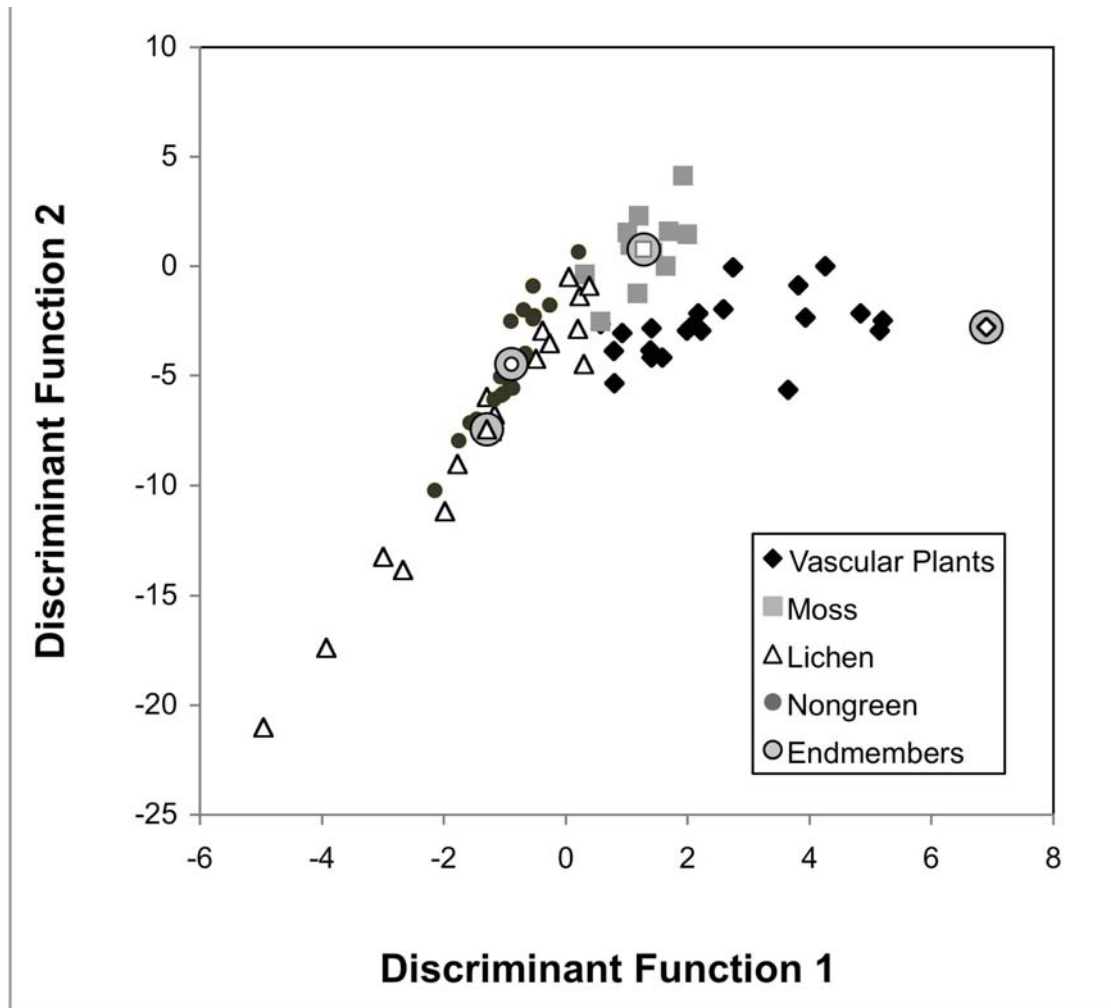
1 **Figures**

2
3 Figure 1. Absorbed PAR and gross photosynthesis for the three vegetation functional
4 types from plot data collected July 20 and August 5, 2001. Light use efficiency for each
5 functional type was calculated from these data as the slope forced through the origin. See
6 Table 1 for description of regressions.

7



1
2 Figure 2. Endmember spectral reflectance for each cover type, vertical lines indicate
3 wavelengths used in the discriminant analysis.
4



1
2 Figure 3. The distribution of data from plots using the first two functions derived from
3 discriminate analysis for the three vegetation functional types and nongreen materials.
4 The larger gray circles indicate values used as endmembers in the unmixing analysis. For
5 the endmember points the symbol within the circle indicates the vegetation functional
6 type of that endmember.

7

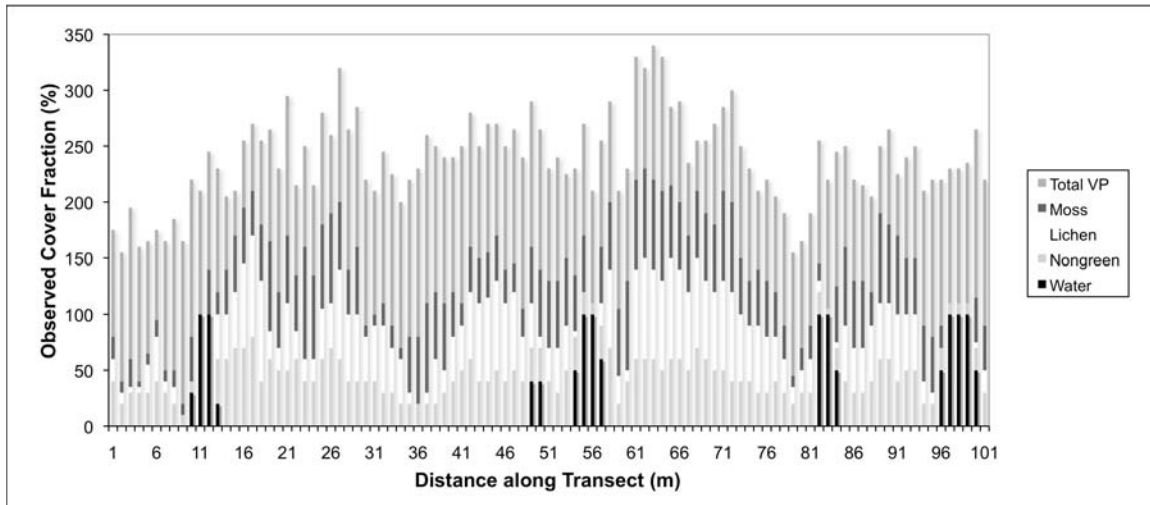


Figure 4. Observed functional type coverage at 1 m intervals along the transect, visually estimated over the period August 8-11, 2001. Because the vegetation is 3-dimensional, total cover fractions were over 100%. In the data analysis the total cover fractions were normalized to equal 100%.

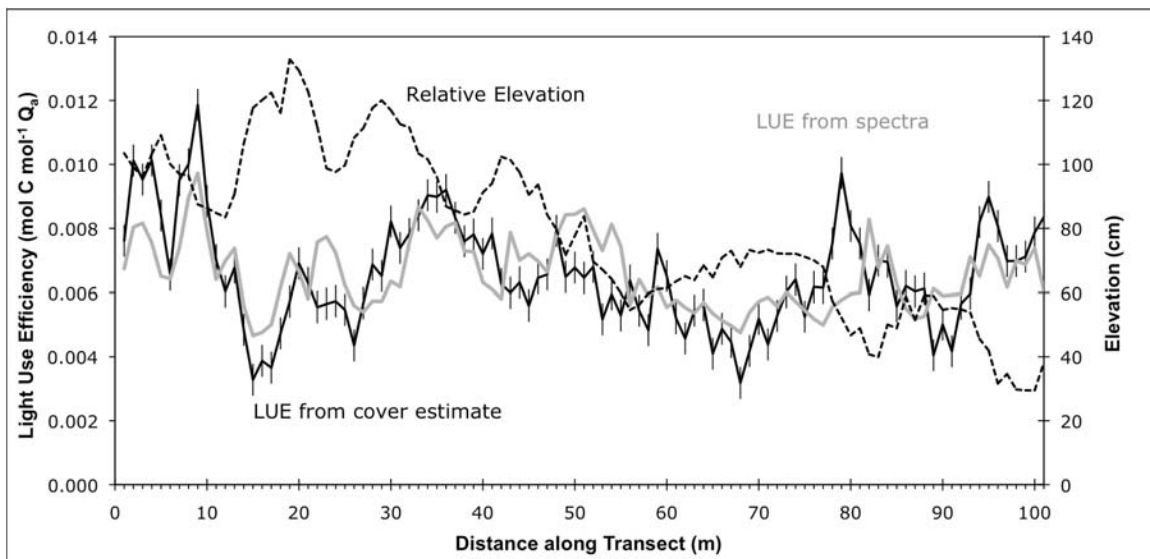
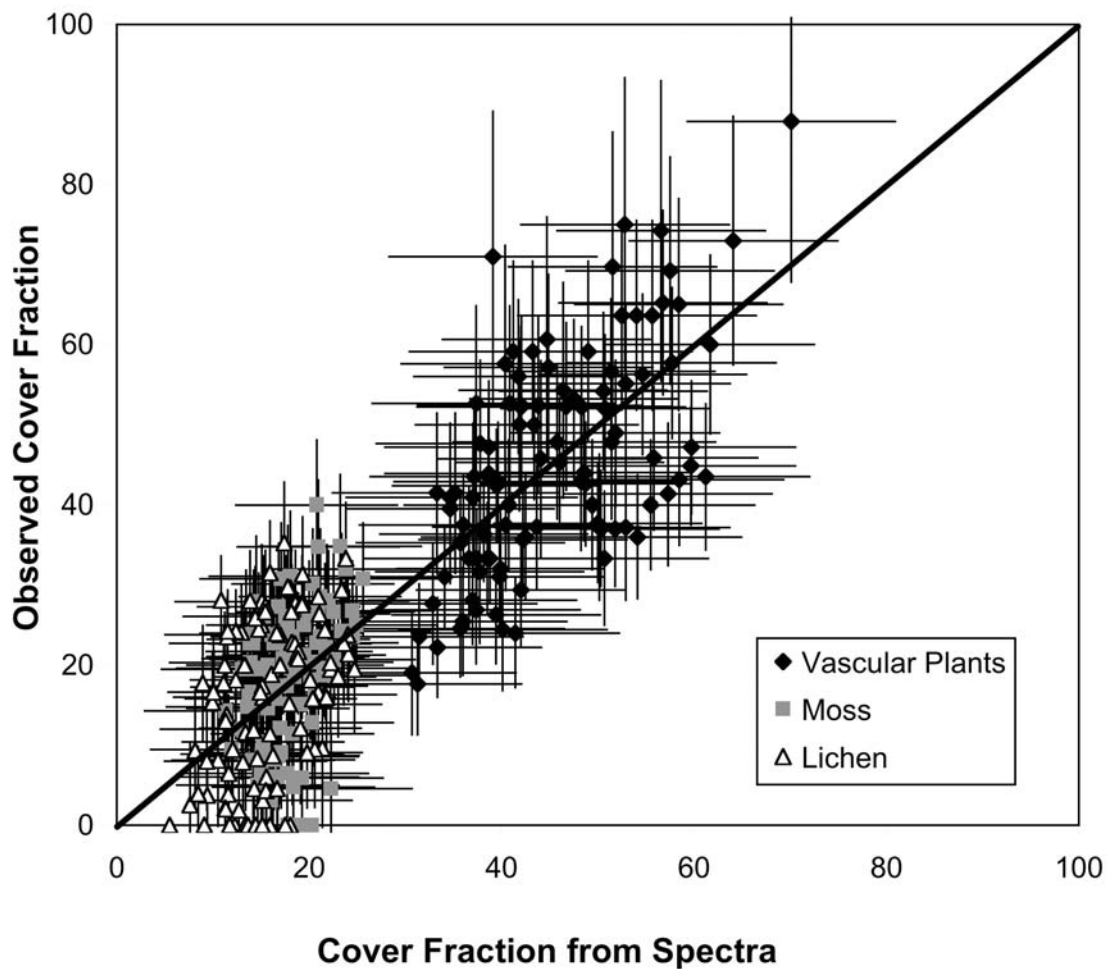


Figure 5. LUE along the 100 m transect shown with the black line was estimated from the functional type coverage (shown in Figure 4) and light use efficiency (shown in Figure 1), along with LUE estimated using coverage derived from spectral unmixing shown with

- 1 the gray line. Microtopography is shown as dashed line. Error in Observed LUE estimate
 2 is $0.00136 \text{ mol C mol}^{-1} \text{ quanta}$, RMSE in LUE derived from observations compared to
 3 LUE from spectra is $0.00266 \text{ mol C mol}^{-1} \text{ quanta}$.

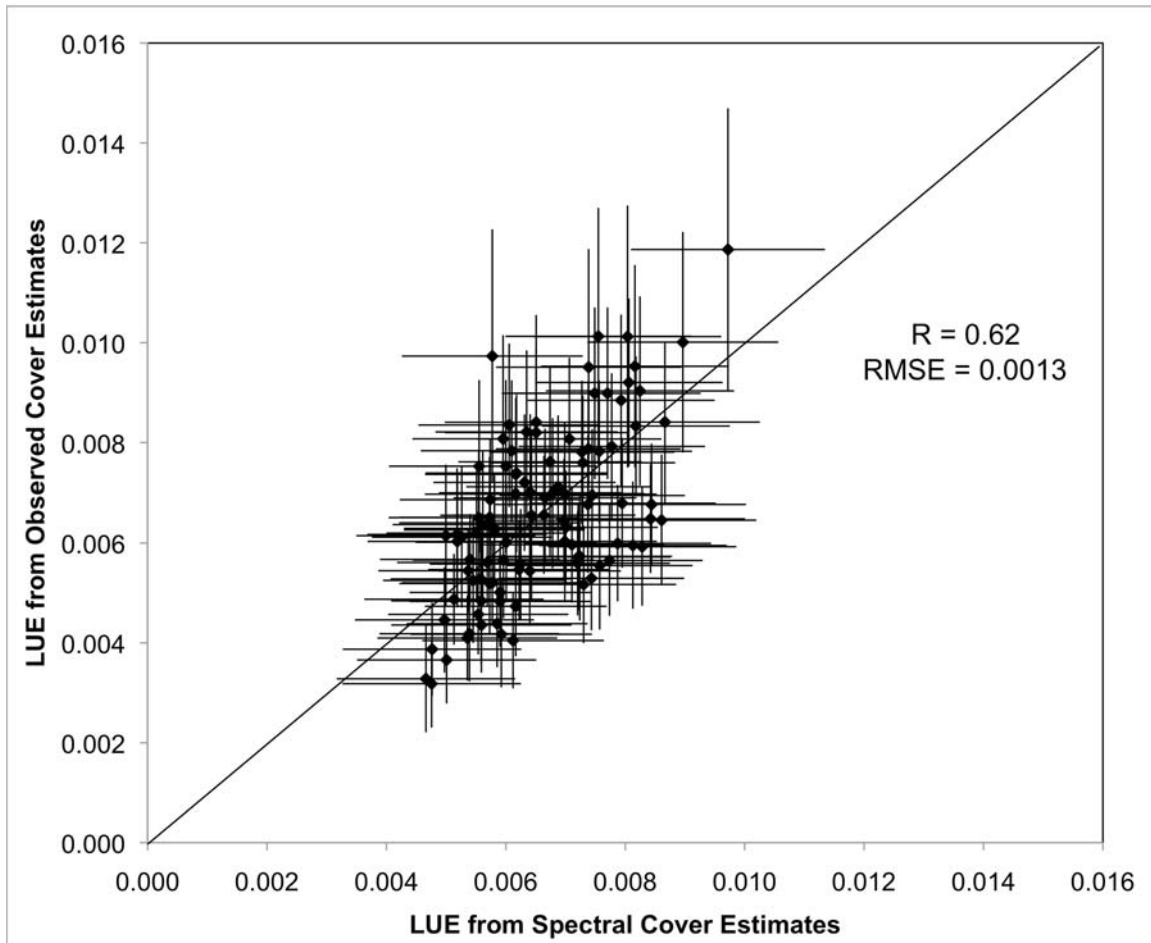
4



5

- 6 Figure 6. Comparison between observed vegetation functional type coverage normalized
 7 to 100% for vascular plants, mosses, and lichens along the transect and cover fractions
 8 estimated from spectral reflectance. Line is 1 to 1 line. The absolute error in visual
 9 estimates is approximately 9%. The RMSE of spectral retrievals is 9% absolute.

10



1

2 Figure 7. LUE (mol C mol⁻¹ quanta) along the transect estimated based on observed
3 normalized cover fractions and cover fractions obtained from spectral unmixing. Line is
4 1 to 1 line. Errors in LUE based on observed cover fractions are due to errors in LUE for
5 the pure functional types and an assumed 15% error of observed raw coverage amounts.
6 Errors in LUE based on spectrally derived cover fractions are due to errors in LUE for
7 pure functional types and the RMSE of the spectral retrieval of cover fractions.

8

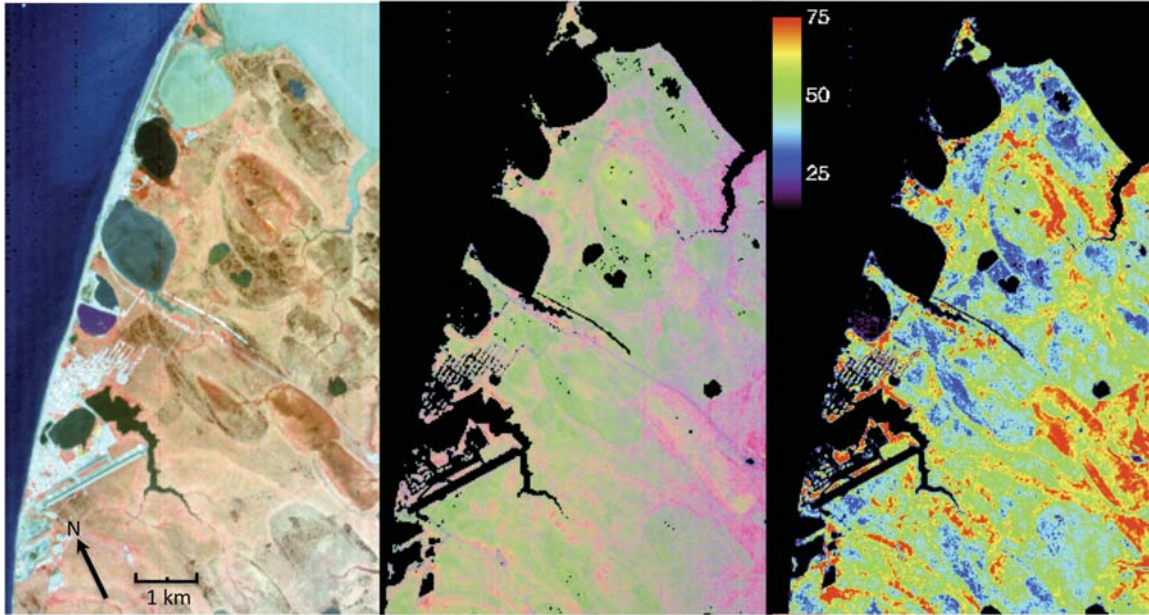


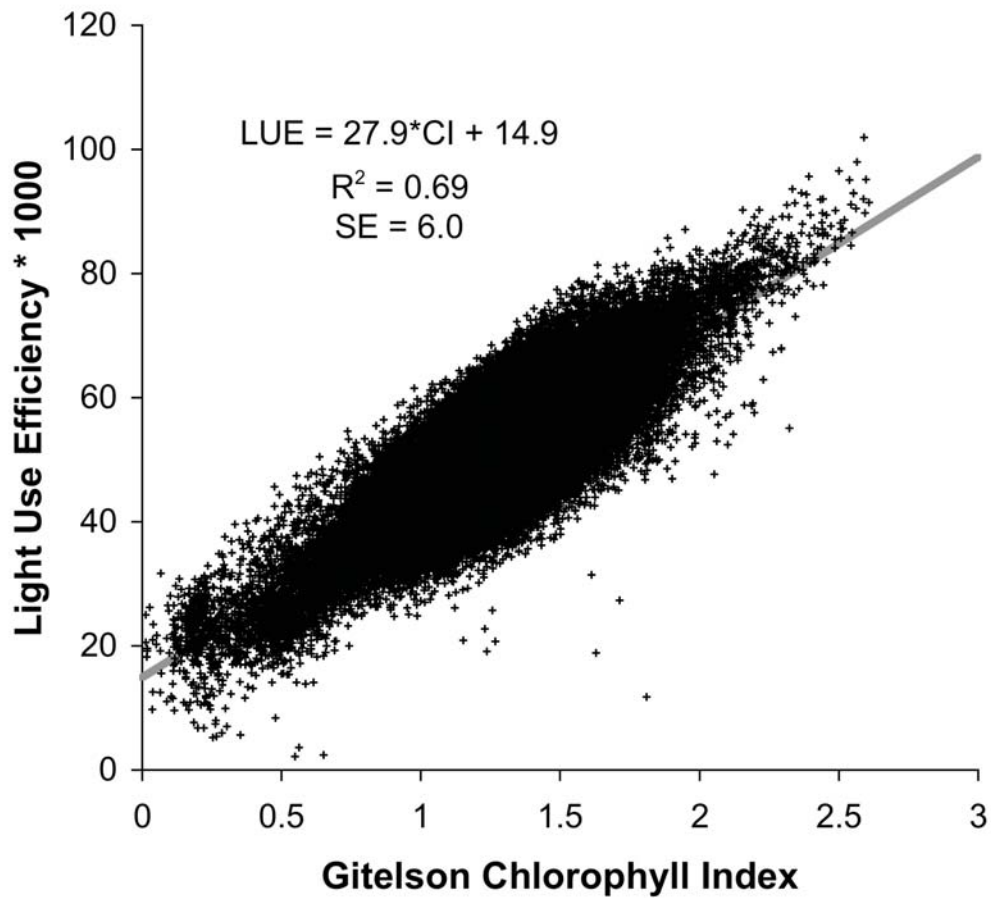
Figure 8. Three versions of the EO-1 Hyperion image acquired on July 20, 2009 are shown.

Left: 3-band (RGB=834, 671, and 549 nm) composite image of surface reflectance. The grid of light blue lines on the lower left side of the image is the city of Barrow. The straight blue line along the shore near the top of the image is the old airport runway, used in the error evaluation. The oblong features scattered around the region are drained thermokarst lakes and the dark red ones are now marshes.

Middle: Three band RGB continuous fields of estimated coverage of vegetation functional types derived from spectral unmixing and scaled between 0 and 50% coverage.

R = Vascular Plant Cover, G = Moss Cover, B = Lichen Cover

Right image: Map of LUE spatial patterns ($\text{mol C mol}^{-1} \text{ quanta} \times 1000$) based on coverage estimates.



1

2 Figure 9. Scatter plot of chlorophyll index (x-axis) versus LUE (mol C mol⁻¹ quanta
3 x1000) based on normalized cover fractions (y-axis). Both variables were retrieved from
4 the Hyperion image.

5

1 Author Biographies

2



Karl Fred Huemmrich received a B.S. degree in physics from Carnegie-Mellon University and a Ph.D. in geography from the University of Maryland College Park. He is currently a Research Associate Professor in the Joint Center for Earth Systems Technology at the University of Maryland Baltimore County. He has developed and used models of light interactions with vegetation, and has studied the use of remotely sensed data to collect information on biophysical variables and land cover type using both computer models and field

measurements. His research has involved fieldwork in a variety of habitats including working on operations and data analysis for the Boreal Ecosystem and Atmosphere Study (BOREAS) and the First International Satellite Land Surface Climatology Project Field Experiment (FIFE).

15



John A. Gamon received his B.S. Degree from Yale University (1979), and his Ph.D. degree from U.C. Davis (1989). Currently, he is a Professor in Earth & Atmospheric Sciences and Biological Sciences at the University of Alberta (Edmonton, Alberta, Canada). His current research involves remote sensing of vegetation function, physiology, and biodiversity.

24

[no picture]

Craig E. Tweedie was born and raised in Brisbane, Australia, and received all of his university level training at The University of Queensland, graduating BSc, BSc (hons) and a PhD in Botany in 1992, 1995 and 2000 respectively. Between 2000 and 2005 he was employed by Michigan State University as a visiting research associate where his passion for Arctic and functional ecological research and international scientific networking was established. He is presently Associate Professor at the University of Texas El Paso in the Department of Biology and the Environmental Science and Engineering Program, and he leads the Systems Ecology Lab.

34



Petya K. Entcheva Campbell (M'99) obtained a BS in Forest Engineering and Silviculture from the University of Forestry, Sofia, Bulgaria; MS in Forest ecology from UMASS Amherst, MA and Ph.D. in Forest Analysis/Remote Sensing from UNH, Durham, NH. Currently she is a Research Assistant Professor at the Joint Center for

Earth Systems Technology, UMBC. She is affiliated with the Department of Geography and Environmental Systems at UMBC, where she has taught GES481/681 undergraduate/graduate classes in “Remote sensing for environmental applications”. She is a research associate at the Biospheric Sciences Laboratory at NASA Goddard Space Flight Center (GSFC), Greenbelt, MD.

Her research focuses on remote sensing of vegetation bio-physical parameters and function for assessing ecosystem processes and dynamics, conducting spectral reflectance and fluorescence analyses and using satellite, airborne, field and laboratory measurements. At GSFC she contributes to the research of spectral bio-indicators of vegetation function, and participates in the Mission Science team for the Earth Observing 1 (EO-1). Dr. Campbell is a member of American Society for the Advancement of Science (AAAS), Geoscience & Remote Sensing Society (IEEE GRSS), International Association for Landscape Ecology (IALE), Society of American Foresters (SAF), and has previously served as the Technical Secretariat for the WGCV/CEOS.



David R. Landis is a Senior Programmer with the Biospheric Sciences Laboratory (Code 618) at NASA/GSFC, Greenbelt, MD. He is currently working on the Earth Exploring One (EO-1) satellite. Mr. Landis has over 25 years of experience as a contract staff programmer-analyst at GSFC. He has experience working for MODIS, Landsat, and EO-1. His information technology experience is extensive, having worked on data systems and data publication tasks for five large climatology projects (FIFE, BOREAS, BOREAS Follow-on, SAFARI 2000, ISLSCP-2). He has considerable programming skill and Web designer experience. He also has significant science background, and has worked with scientists in many disciplines. He received the B.S. degree in Computer Programming from Elizabethtown College.



Elizabeth M. Middleton received a B.S. degree in Zoology from the University of Maryland in 1967, the M.S. degree in Ecology from the University of Maryland in 1976, and the Ph.D. degree in Botany from the University of Maryland in 1993.

Dr. Middleton is a Senior Scientist with the Laboratory for Biospheric Sciences (new Code 618) at NASA/GSFC, Greenbelt, MD. She is currently the Mission Scientist for the Earth Exploring One (EO-1) satellite and the GSFC lead for the NASA HypsIRI satellite concept development. Dr. Middleton recently received in 2011 a Career Achievement Award from the Hydrospheric and Biospheric Sciences Laboratory at GSFC. She also received *NASA Group Achievement Awards* in 1983, 1994, 1995 and 2003, respectively, in addition to numerous Performance Awards. She has previously served, and is currently serving, as the Outside Observer on the Mission Advisory Group (2007-2009, 2011+) for a European Space Agency’s Phase A satellite mission concept-- the FLuorescence Explorer (FLEX). In addition, she was a member of NASA/GSFC Carbon Cycle Science Working Group (2000-2007) and the NASA representative to the US Federal Geographic Data Committee’s Vegetation

- 1 Subcommittee for many years. Dr. Middleton leads a research team that studies
- 2 vegetation spectral bio-indicators of plant stress and photosynthetic function, including
- 3 plant fluorescence. She is Associate Editor of *J. Appl. Remote Sensing*.
- 4